DOI: 10.13009/EUCASS2022-4784

Development of an Inertial Particle Separator Test Facility for Air-breathing Aircraft Systems

HEE Jee Loong*, BOJDO Nicholas**, OZER Ozgun, QUINN Mark, FILIPPONE Antonio
The University of Manchester
Oxford Road, Manchester, M13 9PL, UK
*jeeloong.hee@manchester.ac.uk, **nicholas.bojdo@manchester.ac.uk

Abstract

Inertial particle separators are fitted to intakes to remove foreign particles by action of drag and bounce, and the implementation of a scavenge channel into the ductwork. This separator design concept was chosen for integration into the fresh-air turbo-compressor intake of a more-electric aircraft. The work describes the design, instrumentation, and initial commissioning of a test facility used to validate numerical simulations of different concept geometries. It is concluded that performance is highly sensitive to core-to-scavenge flow ratio, that flow breakdown occurs at a Reynolds number of around 100,000, as characterised by a jump in scavenge mass flow rate.

1. Introduction

An inertial particle separator is a device fitted to the intakes of air breathing engines to remove foreign object debris, non-aqueous aerosols, and water droplets. Their primary aim is to clean the inbound air in order to protect the rotating turbomachinery and associated components from premature damage. They are commonly found on aircraft that operate more frequently from unprepared landing sites, such as helicopters and short take-off military turboprop aircraft, and work by forcing particle-laden air around a bend before bifurcating the flow into clean (core) and dirty (scavenge) channels [1].

A European Union Horizon 2020 innovative project called *A New Technology Innovation for Foreign Object Debris removal* (ANTIFOD) has been established to develop a prototype of an intake protection system for the turbo-compressor of a more-electric aircraft air management system. In such an architecture, the air used for cabin pressurisation is taken directly from the atmosphere external to the aircraft, mitigating the need to bleed air off the turbofan engine compressor stage; hence improving the overall efficiency and reducing fuel burn. However, removing the turbofan and several stages of compressor from the pathway of fresh air to the cabin, leaves the replacement compression system vulnerable to erosion, corrosion, and structural damage by ingested particulates, water and foreign object debris, severely shortening its working life. The major challenge of this project is to develop a protection system that extends the turbo-compressor maintenance intervals to reasonable levels within a strict pressure loss budget, and across a wide range of atmospheric conditions. The design requirements are quite unique in comparison to prior art, thereby necessitating a fresh approach to particle separator design.

To enable the necessary investigations, a new testing facility for particle separators of this scale and application has been developed. The present work discusses the design of an experimental rig whose test section is a scaled two-dimensional planar particle separator geometry which was designed to permit full optical access for flow visualisation and two-phase particle image velocimetry studies. The 1:2 scale rig has been sized to replicate duct Reynolds numbers of the full-scale geometry at the key operating points. The test section housing is designed to accommodate additive-manufactured multi-pipe configurations and facilitate investigations of span-wise flow on particle separation, as depicted in Figure 1. Within this contribution we present the capabilities of the facility, demonstrated using a well-characterised geometry from the literature.

2. Equipment and Test Facility

The ANTIFOD particle separator test rig is housed at the University of Manchester Department of Mechanical, Aerospace, Civil and Engineering (MACE). The test rig consists of 6 main subsystems: particle delivery system (PDS), inertial particle separator test section (IPS), pleated particle filtration system, flow-metering devices, flow controllers and finally the air delivery unit. An isometric view of the assembly is shown in Figure 1.

DOI: 10.13009/EUCASS2022-4784

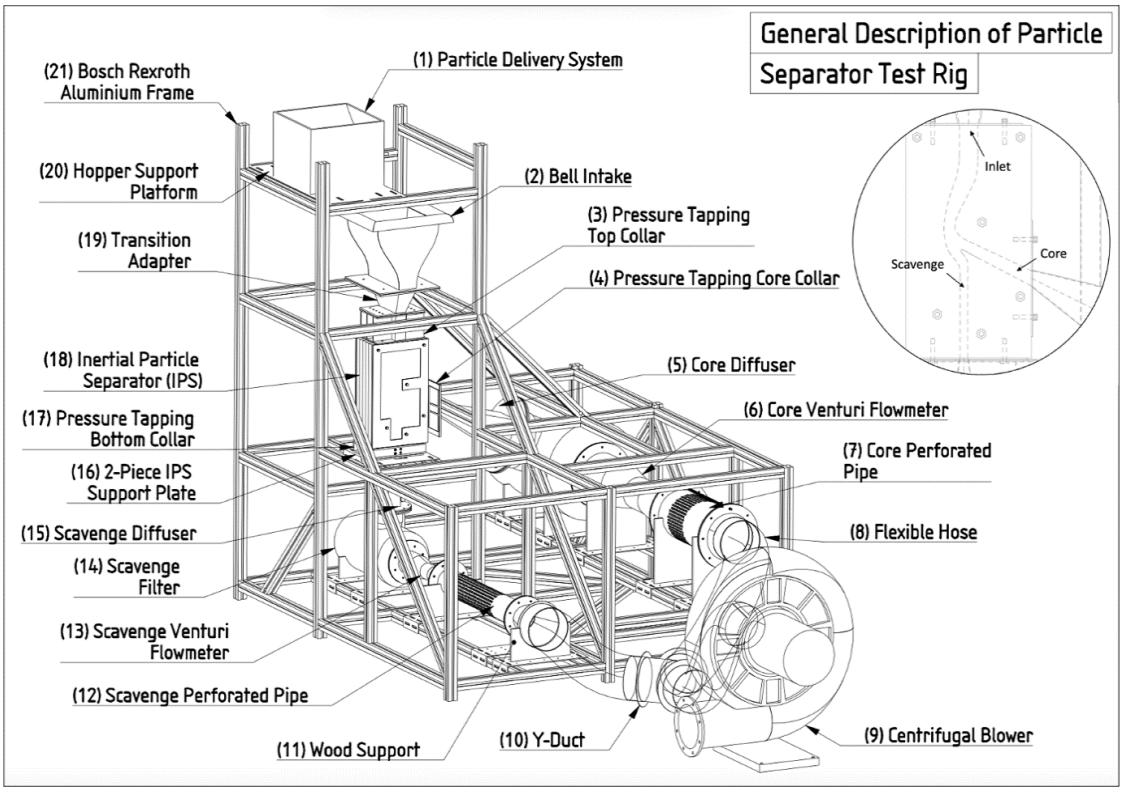

Figure 1: Isometric view of particle separator test rig

With reference to Figure 1, PDS is located above the bell-intake where its weight is supported by aluminium struts and plates, and a Kern 30 kg weighing balance with 1g precision for monitoring delivery dust mass. The bell intake is designed based on a polynomial curve taken from a literature to provide low turbulence level and reduced entry loss [2]. Between the bell intake and the IPS housed a pressure tapping collar used for measuring the static pressure at the respective location. This reading with subsequent pressure readings embedded in the subsystems allows determination of pressure drop across the whole system. In the mid-section of the test rig is an Inertial Particle Separator (IPS). The cross-sectional view of the IPS is shown in an inset image in Figure 1. This inset image shares similar viewing perspective as how a high-speed camera will perceive, where it will be placed perpendicular to the optical window.

Moving along the gas path within the IPS, the bifurcation zone splits the channel into two channels, namely, scavenge passage and core passage. A different split ratio is usually applied to achieve the desired flow conditions. The core passage is the location where it is usually connected to a turbomachinery (i.e., compressor), whereas the scavenge passage is connected to a secondary channel, which in practical contexts exhausts particle-laden 'dirty' air overboard. To smoothly transition the area of the IPS's outlets with the inlet of particle filters, diffusers are used. The particle filtration devices are designed in accordance with ISO *5011:2020* standard and it serves to measure the IPS gravimetric efficiency. The volume flow rates across the channels are measured using Venturi flowmeters as labelled in the diagram. These are connected to 'mechanical' perforated pipes which act like a flow controller valve. These perforated pipes are used to vary the flow rate by exposing a variable number of holes to the atmosphere. Downstream of the flow controllers is a Y-duct which unifies the channels into a single suction source (of the centrifugal blower). The overall structure of the test rig is made up of standard of-the-shelf *Bosch Rexroth* aluminium profiles. Details of the sub-system and engineering justifications are provided in subsequent sections in this paper.

2.1 Intake Design

Air intake shape is critical in achieving high flow quality at the experimental test section and to reduce entry losses. Poor intake design also affects the particle distribution and promotes turbulence fluctuation causing unreliable measurement downstream of the intake. To achieve lower turbulence level and more uniform flow, the shape function for the intake contraction unit is taken from work of Kao *et al.* [2]. The proposed contraction equation used for generating the surface of the ANTIFOD's bell intake is provided as following:

DOI: 10.13009/EUCASS2022-4784

$$y = \left(-6\left(\frac{x}{L}\right)^5 + 15\left(\frac{x}{L}\right)^4 - 10\left(\frac{x}{L}\right)\right)(H_i - H_o) + H_i \quad \textbf{(1)}$$

Where, x is axial distance along the intake central axis, L is the contraction length, H_i is the inlet height from centre axis and H_o is the exit height from centre axis. A 2-dimensional plot of the intake cross-section is provided in Figure 2. The inlet area is set as 300 mm × 300 mm and the outlet area as 300 mm × 81.6 mm. This yields a contraction ratio of 3.676 (based on the ratio of inlet area divided by outlet area of the bell intake). An intake depth of 300 mm is used to maintain an aspect ratio of 1:1. For initial tests, it was decided that a 1:2 scaled IPS should be used to utilise the pre-existing blower in the lab. Therefore, an additional adapter is further re-introduced at the bell mouth outlet to transition the area from *300 mm × 81.6 mm* to *150 mm × 41.3 mm*. The length of the adapter is set as 125 mm. An illustration of the bell intake and the transition adapter are shown in Figure 3.

As the surfaces across the bell intake and the adapter are no longer smooth and continuous, 3D-printed inserts are implemented on the side walls to minimise the tendency of flow separation. These inserts are indicated by the label *'Bezier curve'*. This implementation smoothens the transition on the walls as shown in Figure 4. The final contraction ratio is 14.5.

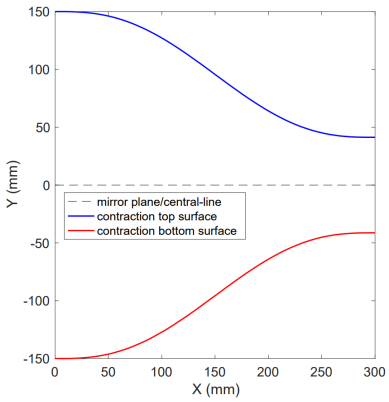

Figure 2: 2D plot of bell intake

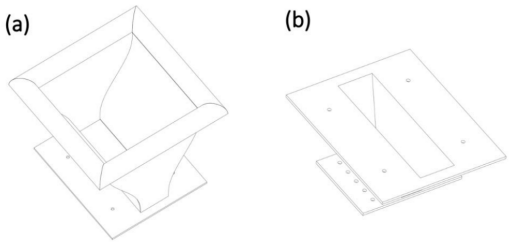

Figure 3: Sketch of (a) bell intake and (b) transition adapter

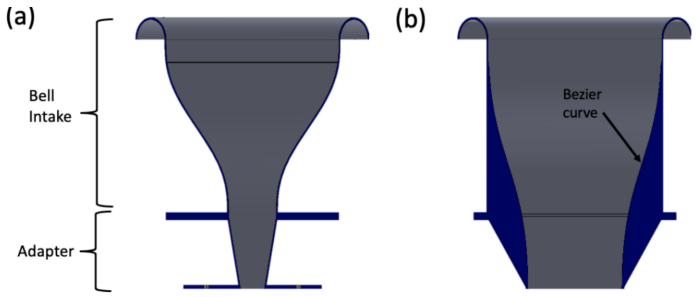

Figure 4: Cross-sectional views of bell intake combined with adapter transition piece
(a) Side view 1 (b) Side view 2

2.2 Test Section & Pressure Tappings

The 2-Dimensional particle separator geometry of Barone *et al.* is used as a reference guideline for the rig development [3], in order to validate a low-order IPS code developed at the University of Manchester, the numerical simulations used to design the 1:1 scale proprietary geometry of the project, as well as to develop a prototype testing facility. A planar sketch of the 2D IPS based on the Barone *et al.* [3] is shown in Figure 5.

In terms of manufacturing of the particle separator test section, a 'sandwich' approach is adopted. The 'sandwich' approach can be referred to as a manufacturing and assembly of various blocks of similar geometric component in the spanwise direction to achieve the final desired geometry. As opposed to a single unibody construction, there are distinctive advantages and disadvantages. The following key points describe the pros and cons associated with this method. The *advantages* are as following:

DOI: 10.13009/EUCASS2022-4784

- Ease of construction based on conventional Coordinate Numerical Control (CNC) machining to create the IPS internal and external profiles
- Sandwich method allowing aluminium and light-permitting *Perspex* block to be bundled together providing excellent optical access for PIV and laser
- Thin *Perspex* window (or viewing window) can be added with no/little curvature, therefore providing less image distortion
- Variable width geometry enables end wall effect to be investigated providing data for flow behaviour in a small or large separator
- Permitting the measurements of the coefficient of restitution of two materials (i.e., Aluminium & *Perspex*)

The *disadvantages* are as following:

- Minor manufacturing error on a single unit could cause surface non-uniformity in the spanwise direction when fully assembled
- Particle-wall interaction behaviour is different to the actual separator as it typically uses only a single type of material (i.e., Aluminium)

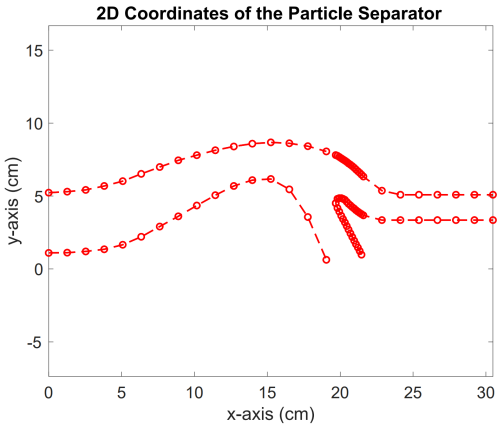

Figure 5: Sketch of IPS as plotted using coordinate points provided by Barone et al. [3].

An image of the fully assembled IPS is shown in Figure 6. In this construction, 30 mm individual block of aluminium and *Perspex* are used. A total of 5 sandwich pieces created the overall IPS of width 150 mm. M8 internal threads are made on 3 faces of an individual block to allow connection with upstream and downstream components. Six silver steel M10 pins are used to secure the sandwich pieces together and metal frames are used to provide structural support due to suspending blocks when the IPS is tilted. During assembly and inspection, surface non-uniformity is observed at the splitter block (this corresponded to the *disadvantages* point). Hence a unibody aluminium single piece splitter block machined using CNC and Electrical Discharge Machining (EDM) is used to substitute all 5 individual pieces solving the surface irregularity issue. An illustration of the unibody splitter block is shown in Figure 6 inset image.

Referring to the cross-sectional view and descriptions provided in Figure 7, the IPS is formed of three pieces, namely, top block which forms the Outer Surface Geometry (OSG) as referred to in Barone *et al.* [3]. The front block forms the bottom wall and hump, rear or splitter block is responsible for segregating the flow into two gas paths (one towards the scavenge and one towards the compressor core). Stacking up aluminium and *Perspex* pieces created the object shown in Figure 6 below.

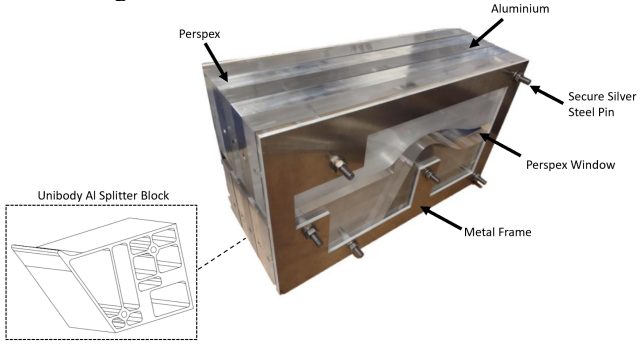

Figure 6: Inertial Particle Separator (IPS) / test section as assembled using threaded pins and nuts

DOI: 10.13009/EUCASS2022-4784

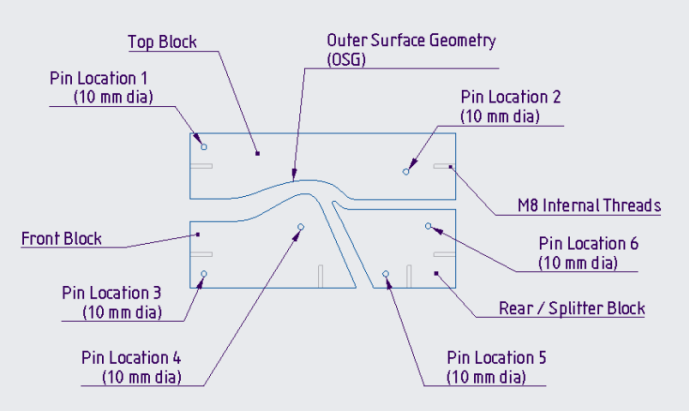

Figure 7: Cross-sectional view and description of a single unit IPS section

To measure the pressure at the IPS inlet and IPS outlets, two 3D printed parts are made using fully filled resin to allow pressure tapping needle to be drilled and inserted normal to the part surfaces. On each block, four pressure tapping holes are made at 2/3 distance away from the inlet or after the exit along the depth of the block. As the bottom pressure tapping block takes the highest mechanical loading due to the weight of the IPS and the upstream components, the tapping block is made from aluminium plates and bars. Illustrations of the pressure tapping blocks are shown in Figure 8. Silicone tubes are used to connect the tapping needles with *Honeywell* pressure sensors to record the pressure readings. Note that, the cross-sectional areas of the pressure tapping blocks are kept constant to prevent pressure variation or velocity variation.

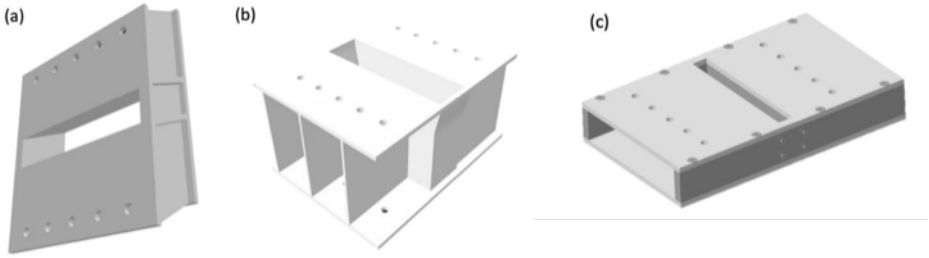

Figure 8: Images of pressure tapping blocks (a) Top section (b) Core section (c) Scavenge section.

2.3 Diffusers / Transitioning Duct Work

To transition the cross-sectional areas of the IPS outlets with the filter inlets, a diffuser is inserted between the two components. This reduces the flow velocity sufficiently without causing flow separation which could increase the pressure drop across of the system. The diffusers are designed based on general engineering guideline provided in the fluid mechanics textbook by White [4]. Key parameters of the diffusers' design are provided in Table 1.

Table 1: Key dimensions for core and scavenge diffuser

	Core	**Scavenge**
Inlet Area, A_1 (m^2)	0.0047	0.0026
Outlet Area, A_2 (m^2)	0.0271	0.0052
Area Expansion Ratio (A_2/A_1)	5.832	1.986
Diverging Angle (°)	19.6	12.5
Overall length (mm)	400	250

As detailed in Figure 9, the flange for both diffusers inlet is designed as rectangular to match the outlet faces of the IPS block (see Figure 6). Ten 8 mm holes are located on each flange faces to ensure perfect alignment with the IPS test section that has ten internal M8 threading on its metal and *Perspex* block. *Ethylene Proplyene Diene Monomer* (EPDM) gasket of 1.5 mm that has cut-out passage is placed onto each of the flange faces to ensure good sealing. At the outlet of the diffuser, a circular flange is added and has eight 8 mm holes equally spaced around the flange at 45° to allow mating with the filter flange. The thickness of each flange is recommended as 6

DOI: 10.13009/EUCASS2022-4784

mm to prevent warping during the welding process. The diffusers are made by welding of all individual pieces. Each of the individual pieces are fabricated using waterjet cutter.

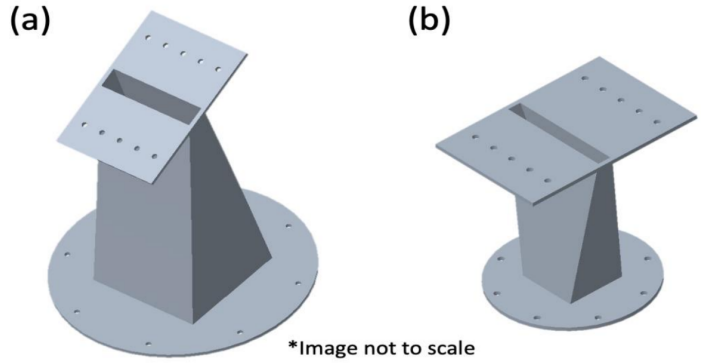

Figure 9: CAD model of (a) Core (b) Scavenge diffusers

2.4 Particle Filtration System for Gravimetric Test

The IPS has two outlets; core and scavenge. To measure the gravimetric efficiency of the IPS for performance testing and to prevent damages to the suction source, the outlets of the particle separator must be installed with a particle filtration system that is capable of capturing particles with 99.5% filtration efficiency (i.e., for particle size of 0.97 microns and above). The ISO *5011:2020* standard is adopted for setting up the filtration system for the test rig. A diagram of the general layout for ISO *5011:2020* standard is shown in Figure 10.

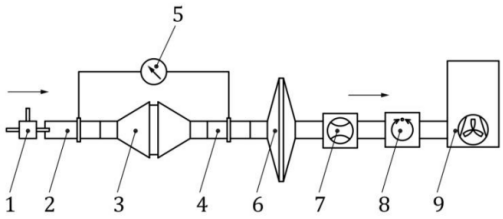

Figure 10: A schematic set-up for performance testing of a filtration system

Where the above labelling refers to (1) dust injector, (2) inlet tube, (3) panel filter chamber (4) outlet tube (5) pressure measuring device, (6) absolute filter, (7) air flow meter, (8) air flow control (9) exhauster. With reference to the Figure 10, the test subject (i.e., IPS) is situated in location 3. The absolute filter (labelled no.6) is responsible for collecting 99.9% of the injected test dust. The only difference in the ANTIFOD test rig is an additional channel and filter. As for performance testing, the particulate mass collected at absolute filter is weighed to obtain the gravimetric efficiency.

Two *Donaldson* ERB2 Pleated Drum Air Cleaners originally designed for diesel engines were used in the ANTIFOD test rig as they capture 99.7% of ISO *12103* A.2 fine test dust when subjected to filtration efficiency test standard of ISO *5011:2020*. For reader information, A.2 fine dust has a size distribution ranging from 1 to 120 μm with a mean particle size of 18 μm. It is worth noting that the fine dust concentration deployed in ISO standard is 1 g/m^3, which is an order of magnitude greater than the concentration planned for the ANTIFOD experiments. Therefore, it is likely that the holding capacity will be reached in a longer time frame.

The key factors used for filter selections are restriction (measured in kPa), air flowrate (measured in m^3/min) and dust holding capacity (g). Oversizing or under-sizing the component could yield poor performance when filter operates under the required operating condition. The restriction is checked to ensure that the blower can overcome the filter resistance and losses due to ducting. Each filter is rated for an optimum operating regime; volume flow rate (VFR). It is important to get a filter suitable for the designed operating condition. For example, the scavenge passage has a lower VFR requirement compared to core passage. The filters selected are *Donaldson* ERB Air Cleaner B100126 (for scavenge) and *Donaldson* ERB Air Cleaner B180017 (for core) respectively. Based on the manufacturer's catalogue, the B100126 model operates optimally when airflow requirement of the scavenge passage is $8 - 14\ m^3/min$. Whereas B180017 works optimally at airflow rate of $32 - 65\ m^3/min$. For filter selection, the maximum operating condition anticipated is taken and the scavenge value is calculated based on the maximum scavenge ratio $\beta = 0.2$. This forms the basis for sizing of components as it represents the maximum operating mode for the test rig. Ideally, it is good to incorporate extra margin (i.e., 20%) in blower sizing to ensure all experimental operating conditions can be met.

DOI: 10.13009/EUCASS2022-4784

The maximum mass flow rate (MFR) at the core and scavenge passage at a flight 'operating' mode are approximately 1.12 kg/s and 0.28 kg/s. As these values exceeded the blower rated capacity, a 1:2 geometric scaling of the IPS is performed. By maintaining the same Reynolds number while reducing the inlet area; the velocity scale across the IPS is effectively increased. The newly derived inlet velocity is approximately 99.39 m/s resulting in a reduced mass flow rate requirement of 0.5589 kg/s and 0.1397 kg/s respectively for core and scavenge passage. The corresponding VFRs are 29.5560 m^3/min and 7.3920 m^3/min. At these prescribed VFRs, the filter surface area is large enough for holding capacity of 60 – 70 hours operation when subjected to ISO Coarse test dust (mean diameter 38 μm) at dust concentration of 0.1 g/m^3. This implies that the pressure drop across the filters is unlikely to rise appreciably during a single 30-minute test run. The ERB Air Cleaner internal media can be removed and replaced when it reaches usage limit.

To ensure that the blower can draw the right amount of air through both filters, the performance curve of Donaldson ERB Air Cleaners from the manufacturer catalogue is evaluated and replotted as shown in Figure 11. Referring to Figure 11, the restriction for core and scavenge filters are 8.6506 mbar and 3.9335 mbar respectively. The IPS is estimated to have a pressure drop of 20 mbar. Based on the blower maximum VFR of 3400 m^3/h, the available pressure is 67 mbar. By deducting the spare pressure with combined pressure drop across filters and IPS, the remaining spare pressure is 34.4 mbar. This provides at least half the pressure headroom for entry losses in bell-intake, diffusers, Venturis, and perforated pipes.

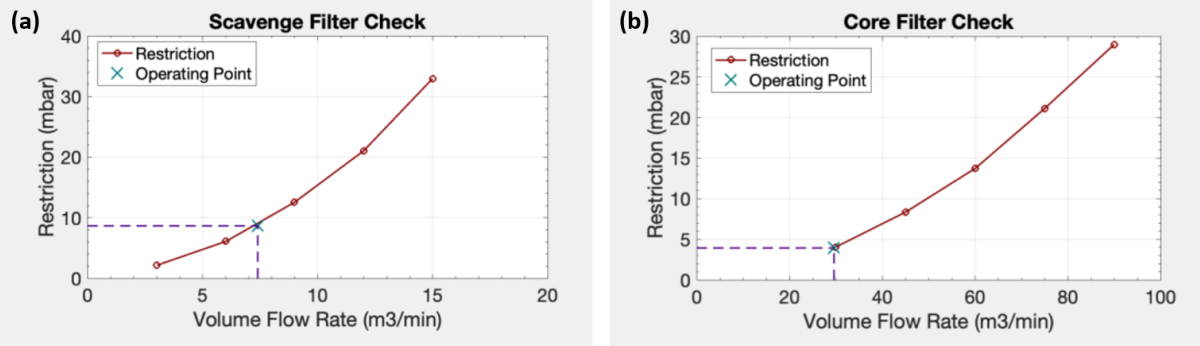

Figure 11: Restriction of (a) Scavenge filter (b) Core filter in mbar with respect to volume flow rate in m^3/min

The images of the core and scavenge filter are shown in Figure 12. The filters have a circular inlet and outlet perpendicular to each other central axis. A removable lid is located at the rear end opposite to the exit where it can be removed for filter media replacement. A rubber seal on the lid prevents air leakages. The inlet and outlet diameters were measured and compared to the value provided in specification sheet, and in-house fabricated aluminium flanges are added to allow connectivity with the diffuser and Venturi. Subsequently, nitrile O-rings are also added at each location to ensure tight sealing. The dimensions for the filters are provided in Table 2 and the labelling can be referred to Figure 13.

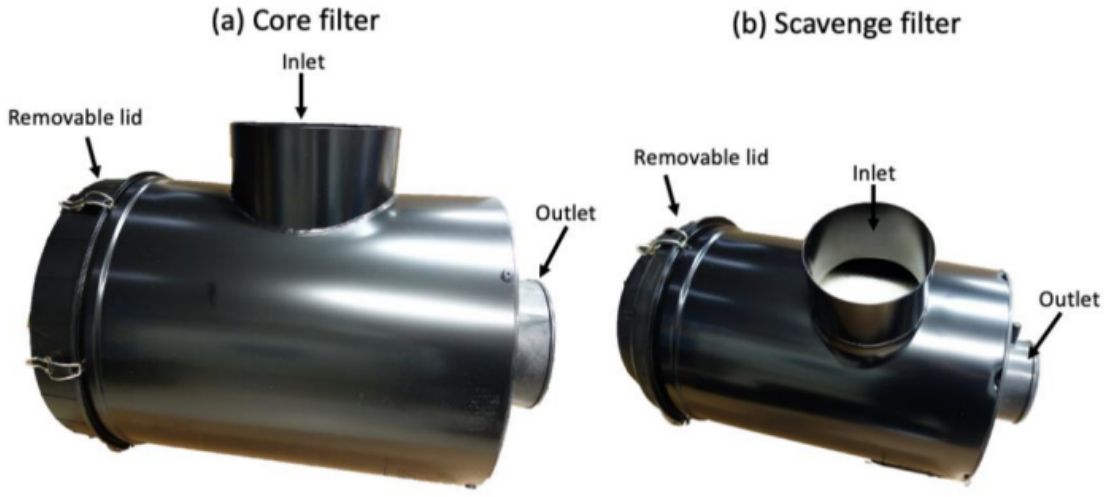

Figure 12: Images of (a) Core (b) Scavenge filter

DOI: 10.13009/EUCASS2022-4784

Table 2: Dimensions of *Donaldson* Air Cleaner B100126 and B180017

Air Cleaner Model No.	Airflow (m^3/ min)	Range Dimensions (mm)									
		A	B	C	D	E	F	H	J	X^o	Z^{00}
B100126*	8 – 14	259	430	114	102	143	52	205	0	400	75
B180017*	32 – 65	457	650	254	203	282	85	328	0	600	130

*Includes safety element X^o free space needed to remove main element Z^{00} free space needed

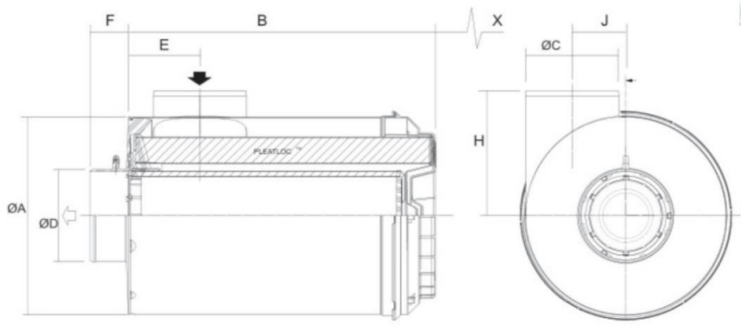

Figure 13: Technical drawing showing a section view of filter B100126

2.5 Venturi Flow Meter

The mass flow rate in the channel is determined using Venturi flow meter. With this information, it is possible to control the mass flow rate in each channel using control valves. Common flow measuring devices in the market are turbine rotary flowmeter, ultrasonic flowmeter, orifice plate, etc. Each has its own features and disadvantages. Due to simplicity and low-pressure loss comparing to orifice plate, Venturi tube is selected for our application [5]. The maximum mass flow rates at core and scavenge channel to be measured are 0.56 kg/s and 0.14 kg/s respectively based on standard air pressure and temperature and the pre-defined scavenge ratio β of 20%. Venturi flowmeter works based on Bernoulli principle where the pressure measured at the entrance and throat and known areas enable the volume flow rate to be determined. The design rules for ANTIFOD Venturi flowmeters are extracted from ISO *5167-4:2003*. The design rules are as follows with reference to Figure 14:

- Throat diameter, d shall be less than $0.224D$ and not greater than $0.742D$, where D is the entrance diameter.
- Length of the throat shall have a length of $1.0d$.
- Cylindrical entrance section shall have an internal diameter D and a length of not less than $1.0d$.
- Conical section shall have a taper of 10.5°. Its length is therefore $2.70(D-d)$ within $\pm 0.24(D-d)$.
- Divergent outlet section shall have an inclined angle of not less than 5° and not greater than 15°. Its length shall be such that the exit diameter is not less than $1.5d$.

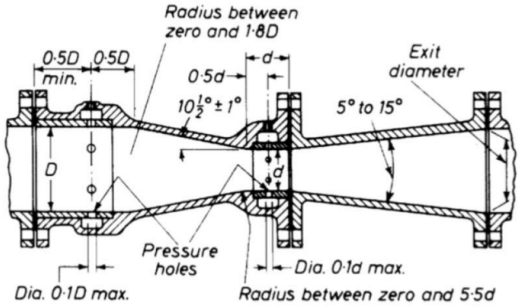

Figure 14: Schematic of Venturi tube taken from Fowles [5].

A Venturi of beta ratio, $\beta_{venturi}$ of 0.7 is used (i.e., ratio of throat diameter to entrance diameter). Typically, a $\beta_{venturi}$ ranging from 0.4 to 0.7 is recommended. The entrance and throat diameter for both tubes used in ANTIFOD test rig along with other parameters are provided in Table 3. A sketch of the Venturi flow meter (core) is provided in Figure 15. Three pressure tapping tubes are inserted circumferentially around the entrance section at a distance of at least $1d$ away from the converging section as suggested by ISO standard. [5]. They are equally

DOI: 10.13009/EUCASS2022-4784

spaced at an angle of 120°. The average pressure is determined across each section using the mean of the 3 pressure tapping ports. Same principle applies to pressure tapping tubes at the throat where 3 pressure tapping tubes are inserted and averaged, the distance of the tapping should be at least $1d$ away from the diverging section.

Table 3: Key aspects of Venturi flowmeter design

Venturi Flowmeter		**Core**	**Scavenge**
Upstream diameter, D	mm	203	102
Throat diameter, d	mm	142.1	71.4
Convergence section length, l_{conv}	mm	164.29	82.55
Divergence section length, l_{diverg}	mm	269.84	135.58
$\beta_{venturi}$ (d/D)	-	0.7	0.7
Converging Angle	°	21	21
Diverging Angle	°	15	15
Number of pressure tapping	-	6	6

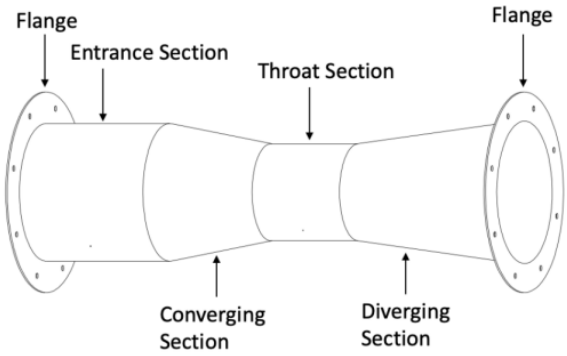

Figure 15: Sketch of the core Venturi flowmeter

2.6 Suction Source / Centrifugal Blower

To deliver the required air up to 0.7 kg/s to the test section, a fan is needed to move the air from the bell intake through the IPS, diffusers, filters, flowmeters and finally vent it back into the ambient environment. To draw particles and air into the system, a suction configuration is deployed where the blower suction side is connected to the test section outlets.

A centrifugal fan is used in ANTIFOD test rig as it provides high pressure air. Centrifugal fan consists of an impeller within a casing that have spiral shape contour. As the impeller rotates at high speed, centrifugal force is generated. Air within the impeller vicinity gain momentum and is discharged outward at the impeller outer periphery. Due to conservation of mass and momentum, the air from the atmosphere is drawn into the impeller axially at the so called 'eye', negative pressure zone is generated there. This continuous operation is what drives the movement of air. Centrifugal fan provides sufficient pressure to overcome resistance at duct, elbow, filters.

Referring to Section 2.4, the pressure drop for filters at VFR 29.55 m^3/min and 7.39 m^3/min are 8.65 mbar and 3.93 mbar respectively. The centrifugal blower used is *Garner Denver* REL62050. With reference to the blower performance curve taken from the spec sheet (see Figure 16), the maximum pressure of the blower at maximum flow rate is 67 mbar. This leaves a spare pressure of 54.42 mbar after deducting filter resistance 12.52 mbar. Subsequently, the IPS is estimated to have a pressure drop of 20 mbar yielding final spare pressure of 34.42 mbar. These are used to overcome losses in bell-intake, diffusers, Venturi tubes and ducting.

2.7 Mass Flow Controller

Due to limited resources, a single centrifugal blower is used for both core and scavenge passages. The centrifugal blower is kept at its maximum operating VFR of 3400 m^3/h and mechanical flow controllers were developed and deployed to control the VFR on each channel. The mechanical flow controller involves the use of perforated pipe and sleeve covers. Illustrations of the components (i.e., perforated pipes and metal sleeves) are shown in Figure 17. The flow controller will be updated in future to permit automatic control of fixed flow rates.

DOI: 10.13009/EUCASS2022-4784

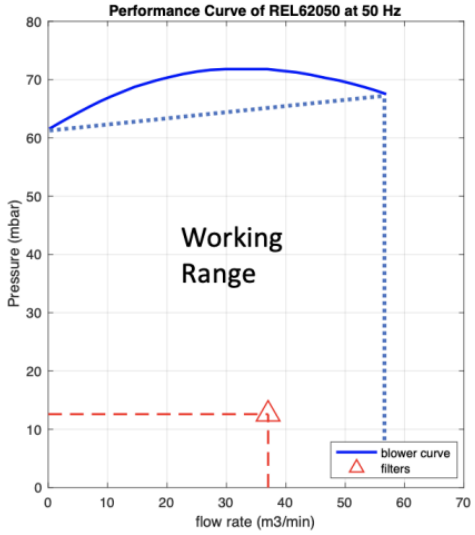

Figure 16: Performance curve of centrifugal blower adapted from *Garner Denver* specification sheet

The perforated pipe contains a series of 10 mm diameter holes spread across the axial length of the pipe, as the holes are exposed to the ambient environment, the below atmospheric pressure inside the perforated pipe which is connected to the suction source will start drawing air in, this reduces the amount of air going through the test section or specifically through core and scavenge passages (i.e., upstream components). Metal sleeves made of aluminium and have semi-cylindrical shape (see Figure 17b) are used to cover the holes when needed. Two-piece sleeves can be joined together to fully form a circular cover that block all holes around the circumferential position of the perforated pipe. The objective of determine the regime map for volume flow rate across both channel, inlet Reynolds number and the achieved scavenge ratio $\beta = 0.2$ based on different sleeves position are provided in subsequent sections.

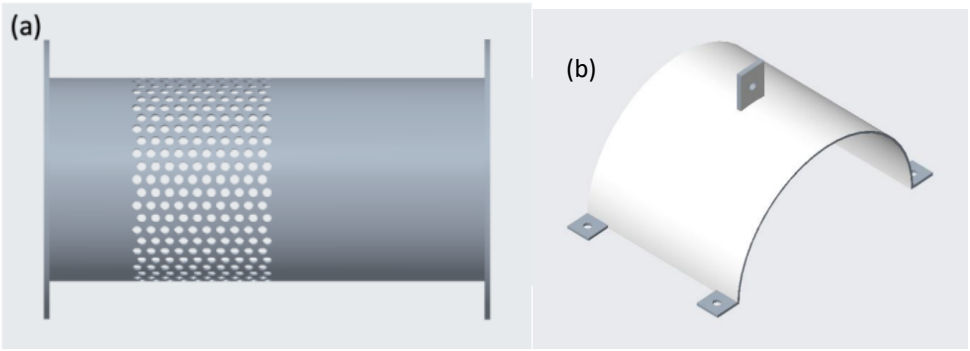

Figure 17: Side view of the perforated pipes (a) core (b) metal sleeve for covering perforated holes.

3. Commissioning and Testing of ANTIFOD Rig

3.1 Calibration of Venturi Flowmeter

Calibration of the Venturi flow meter is necessary to obtain the real volume flow rate across the channel. This is achieved by performing a preliminary PIV experiment where the discharge coefficient (C_d) for the Venturi flow meter equation is obtained by evaluating the inlet velocity of the IPS and work backward to obtain the inlet volume flow rate. Note that Venturi flow meter can also be calibrated using an orifice plate or other known standards. The general formula for Venturi flow meter is as follows:

$$Q = C_d A_{throat} \left[\frac{2\Delta p}{\rho(1-\beta^4)}\right]^{1/2}, \beta = \frac{d}{D} \quad \textbf{(2)}$$

Where, Q is volume flow rate, C_d is discharge coefficient, Δp is the differential pressure across throat and Venturi inlet, ρ is air density, d is throat diameter, D is Venturi upstream diameter. The discharged coefficient obtained using PIV experiment is 0.6. With this data, the operating conditions for the test rig can be obtained.

DOI: 10.13009/EUCASS2022-4784

3.2 Aerodynamic Performance Map Tests

A convention is created to enable the volume flow rate of the flow control devices to be established. These are made on the perforated pipe and subsequently tested to create an aerodynamic performance map or better known as regime map. The following settings were made on the perforated pipe (see Figure 18). Referring to Figure a, six markings on the axial length of the core perforated pipe denoting sixth conventions, namely, C1, C2, C3, C4 and the C6. C1 refers to fully exposed setting where all the bleed holes are uncovered, whereas C6 refers to half covered bleed holes where half of the total exposed holes along the pipe are exposed to the environment. Meanwhile the CF6 is a convention where all the exposed holes are fully covered. This is achieved by using a 360° metal sleeves shown in Figure 18. CF3 refers to using 2-pieces "360 degree" sleeves to cover the holes at the marking location "C3". A similar convention is also adopted for scavenge perforated pipe (see Figure b) for explanation. This varies from S1 to S9 or SF1 to SF9 (note that the full configuration data is not publish here). By sweeping all the test points, an aerodynamic performance map was achieved by altering the inlet Reynolds number, Re and the split flow parameter, β (where these two parameters are a product of the performance mapping exercise). The pressure drop across the IPS is also obtained.

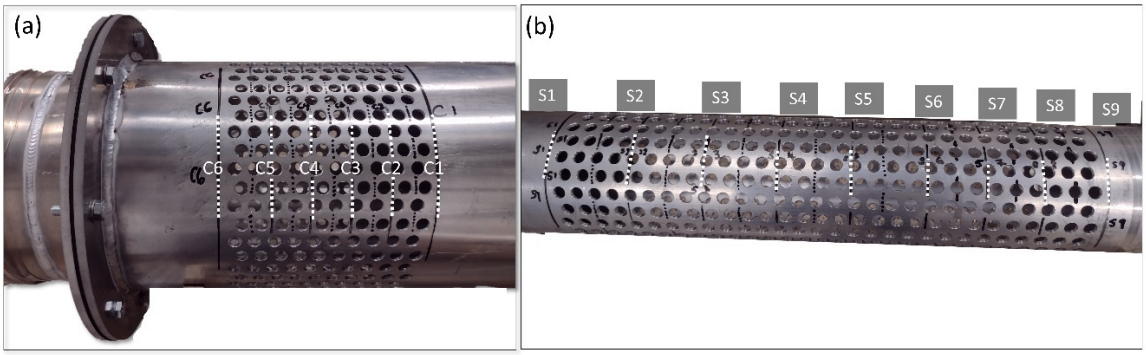

Figure 18: Marking on perforated pipe for flow control: (a) Core perforated pipe (b) Scavenge perforated pipe

Owing to the relative ease of conducting a single test point, it was decided that for a mapping exercise, it would be beneficial to increase the number of test points in order to improve the resolution of the resulting performance curves. A total of 108 test points are recorded for this task. The results of the performance mapping exercise are shown in Figure. It is observable that despite systematically altering the coverage of bleed holes in the mechanical mass flow controller, we see the system respond in a non-linear manner. When the inlet mass flow rate is low, we are able to achieve a range of split flow parameter values with the system. Initially this appeared to be positive outcome – we would like good control of the split flow parameter as an objective. However, the split flow parameter was seen to not increase monotonically will a decreasing number of covered holes. Several outliers were observed, which deviated from the general trend (see Figure 19a). This is believed to be due to the method of measuring mass flow in the scavenge line. We opted to use a Venturi, which performs optimally at its design point, which in this case was when the inlet mass flow rate is around 0.15 kg/s or greater. Since Venturi flow meters rely on calculating mass flow using the difference in static pressure between two points, that arise due to flow acceleration, when the velocity change is very small, fluctations in the reading due to flow unsteadiness can appear magnified. One of the outcomes of this finding is that the scavenge mass flow meter should be redesigned before moving on to the separation efficiency experiement.

It is observable in Figure 19a that as the inlet mass flow increases, the split flow parameter converges on to a narrow range of values between 0.25 and 0.3. This is similar the scavenge to core area ratio at the suction source. We believe that at higher inlet flow rates, the split flow parameter is governed more by the design of the suction source pipework, when the two channels are sharing the same source of suction. The system is always trying to balance the mass flow rate in each leg (core and scavenge), which means that at particularly high flow rates the bleed holes in the scavenge leg, and the associated pressure loss, is insufficient to prevent the scavenge mass flow tending towards the area ratio of the two pipes at the suction source. The current design of the rig thus affords us much less control of β than originally intended. To reduce β further with the existing setup, an orifice plate was introduced into the scavenge in order to induce a source of pressure loss in the scavenge leg. This helped to achieve low split flow parameter values, but not yet as controlled as desired. The long-term fix to the issue is to replace the Venturi mass flow meter with an orifice plate flow meter, and build in feedback control.

In Figure 19b, the relationship between core pressure drop and inlet Reynolds number (Re no.) is established. An observable feature is the pressure loss rising in a quadratic form with increasing Re no. A peak pressure loss of around 950 Pa at the Re no. of 110,000, which is followed by a drop to a range of 730 – 840 Pa at Re no. of

DOI: 10.13009/EUCASS2022-4784

around 135,000. At the same test points, we see in Figure 20a that the split flow parameter jumps to around 0.4 and 0.5, respectively. Without using a flow visualisation technique such as oil streaks, and without simultanously testing separation efficiency, it is difficult to draw firm conclusions. However, based on phenomena observed elsewhere in the open literature, it is quite likely that this represents the point at which the flow over the hump detaches from the leeward surfaces. This causes a jump in the mass flow reaching the scavenge, because the flow is no longer following the path contours of the core and is drawn into the scavenge instead.

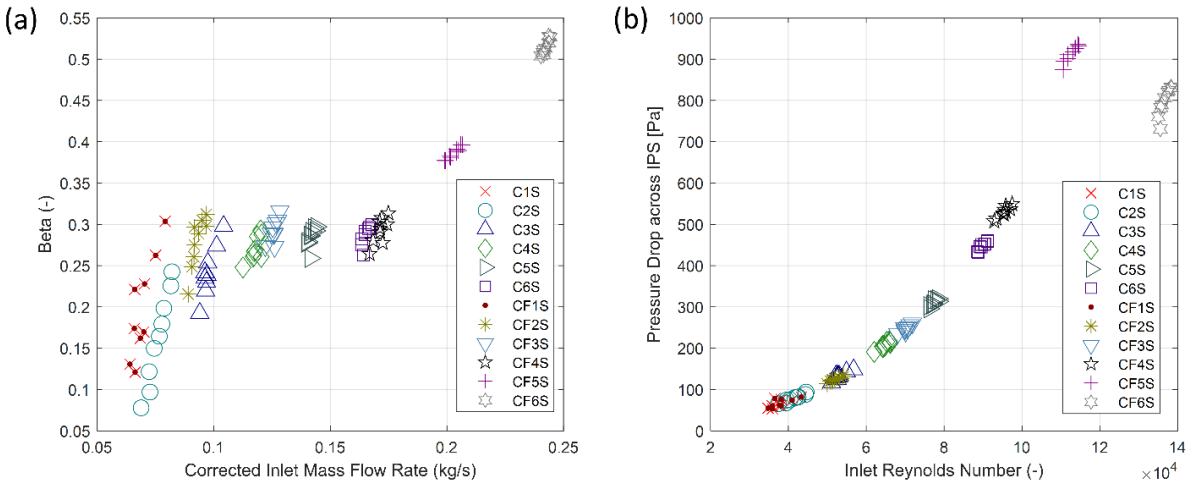

Figure 19: (a) Variation in split flow parameter that can be achieved in the 2D planar rig, over a range of corrected inlet mass flow rates (b) Pressure drop measured between the IPS geometry inlet and the core outlet as a function of inlet Reynolds number.

We believe the flow initially separates at the leeward side of the hump, before separating at the walls, too, to form a bi-modal flow structure across the IPS span – a region of fast flow in the centre of the geometry, a sandwiched between two regions of slow, re-circulating flow in the leeward part of the hump, and laterally at the geometry walls. We believe the slight pressure recovery is owed to the fact that the relatively smaller mass of air entering the core (now just 50%) is not spread across the whole span, and when the flow re-attaches the mean streamwise flow magnitude is slightly smaller than the previous test point. This is a shortcoming of rectangular shaped duct cross sections, such as in the 2D planar test section; corners in the geometry must be left, in order to maintain a clear field of view for the PIV camera. These invariably lead to small interference vortices, which can unsettle the flow. It is not known yet what effect this would have on the separation efficiency, but one would assume that the flow separation, coupled with the loss of spanwise particle separating area, would lead to a reduction. This may be a performance failure mode to be investigated further. More work is required to substantiate these ideas.

In this experiment, the inlet *Re* number is based on hydraulic diameter. We do not manage to reach the intended maximum due to the problem mentioned above. It maybe more appropriate to choose a characteristic length in the *Re* no. calculation that relates more closely to the geometry of the hump (such as its length). This may give us a *Re* no. that we are able to cross-correlate with studies in the literature, in order to verify the behaviour, we are observing. For the purpose of the current study, we continued with the current definition.

4. Preliminary Optical Flow Diagnostics Research

The ANTIFOD particle separator test rig is designed to have optical access for various optical flow diagnostic methods. Particle Image Velocimetry and shadowgraphy methods are tested in the preliminary study.

4.1 Particle Image Velocimetry (PIV)

Particle image velocimetry (PIV) is an advanced flow investigation due to its capability to investigate the whole flow field without creating flow deformations. However, one of the significant drawbacks of PIV measurements at the long narrow channels is the resolution lost due to the aspect ratio difference. The camera sensors are generally manufactured as square or rectangles with a small aspect ratio. So, most pixels capture unintended non-flow containing areas when a long channel with a narrow height is investigated with PIV (Figure 21, red rectangle). As a solution, the investigation area is reduced by compromising some areas of interest (Figure 21, blue rectangle). A stitching stereo PIV is applied to avoid both adverse outcomes, which utilises two simultaneously working

DOI: 10.13009/EUCASS2022-4784

stereo camera setups to capture all areas of interest (Figure 21 (a), blue and purple rectangle). The light sheet passes through the Perspex section of the test section to illuminate the area of interest.

The PIV system consists of a 200mJ ND:YAG Evergreen laser as the illumination source and four LaVision SX4Mpx cameras were mounted with Nikon 50 mm f 1.8D lenses. F8 aperture number is used for all the cameras. The field of view of the cameras is 110 mm x 80 mm, and the time between two pulses of the laser is 30 µs. Each camera captured 500 image-couples with 10 Hz for every design point. These images are cross-correlated and stitched to obtain a single averaged vector map, as shown in Figure 21 (b). A 32px x 32px interrogation area is used for cross-correlation.

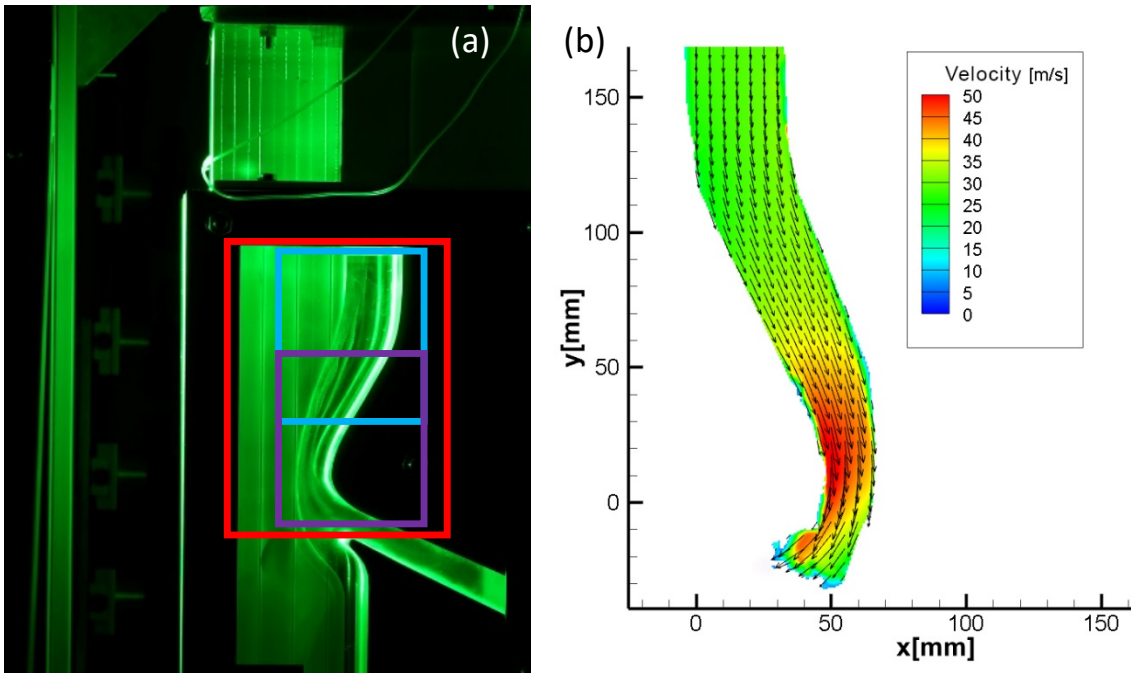

Figure 21: (a) Photograph of the test section during the PIV experiment (b) Sample velocity map obtained by PIV at the area of interest.

The obtained PIV results were utilised for the calculation of the discharge coefficient (C_d) for the Venturi flow meter calibration. Additionally, 14 mass flow controller variations were tested to compare inlet Reynolds number and split flow parameters (Figure 21).

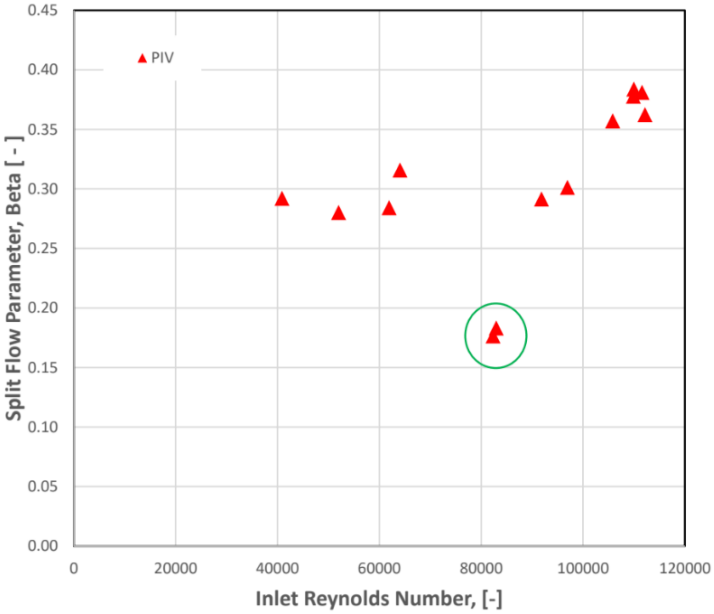

Figure 21: Variation in split flow parameter tested by PIV.

DOI: 10.13009/EUCASS2022-4784

4.2 Shadowgraphy

Shadowgraphy is an ideal method to investigate particle sizes and trajectories. Although it mainly utilises similar equipment as PIV, the optical setup differs. Instead of light sheet optics, a diffuser optic is mounted to the laser to create a collimated light volume. These light rays pass through the test section, and the silhouettes of the passing particles are captured by a telecentric lens (0.9X LF PlatinumTL Telecentric, F-Mt) and a PIV camera (LaVision SX4Mpx) (Figure 22) which is aligned at the same axis with the laser.

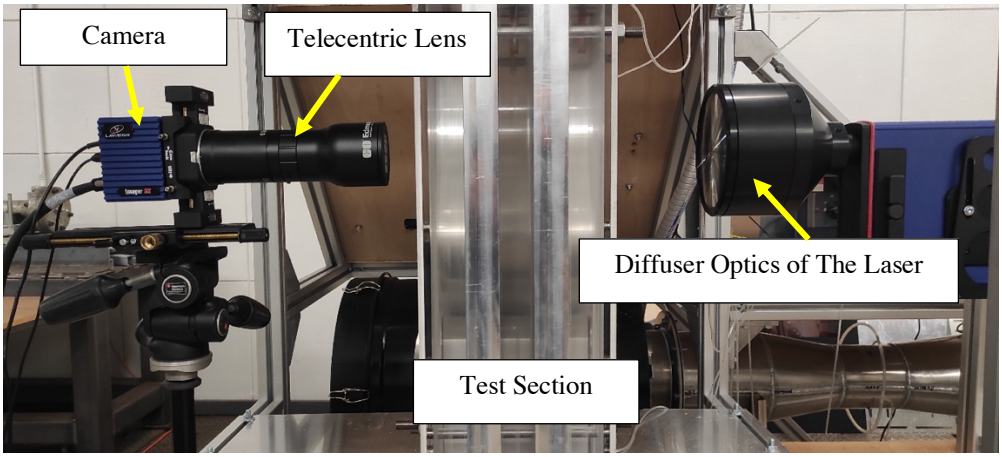

Figure 22: Photograph of shadowgraphy setup with PIV cameras at particle separator test rig

Figure 23 shows a picture-in-picture comparison of an image couple captured during the sand particles test. The time between pulses of laser is 40 µs. The first image is represented by green, and the second image is represented by red. The results show that particle size and shape can be captured clearly in shadowgraphy. Furthermore, the velocity and the rotation speed can be calculated by correlating these images.

An ultrafast camera and diffuse LED light source can also be used as an alternative setup instead of interframe cameras and double-pulse lasers. These cameras can capture with a 10 kHz or faster frame rate, allowing researchers to follow the particles during their travel in the area of interest. This is very advantageous for investigating bouncing particles. However, a continuous light source or a high repetition laser is needed for illumination. The high repetition laser is favourable since the LED light source does not supply fully collimated beams, which results in sharpness loss at the edges and multiple shadows of unfocused particles (Figure 24). In this preliminary stage of the optical flow diagnostics study, various shadowgraphy setups were compared to determine the most suitable options to use at the ANTIFOD particle separator test rig.

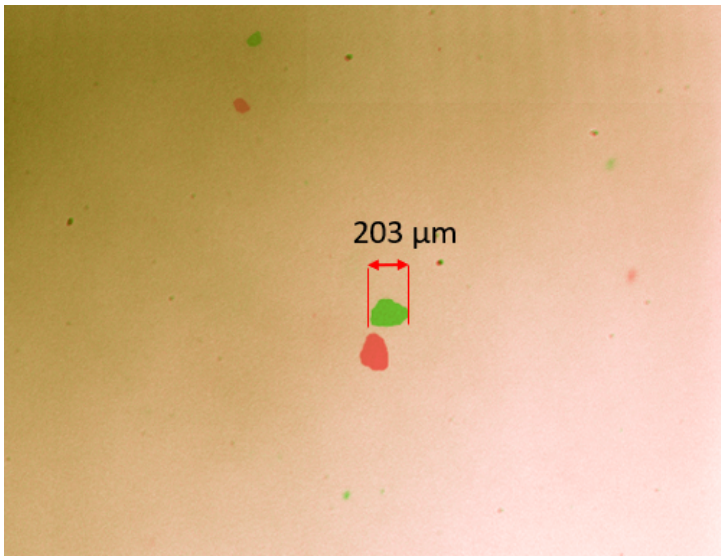

Figure 23: Sample shadowgraphy result obtained by the PIV camera and the laser; picture in picture comparison of an image couple taken in 40 µs; the first image is represented green, and the second image is red.

DOI: 10.13009/EUCASS2022-4784

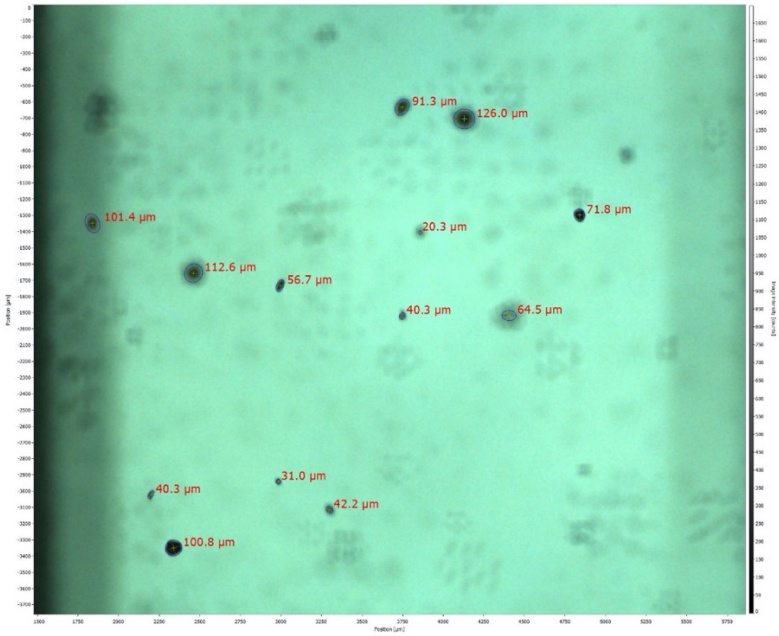

Figure 24: Sample shadowgraphy result obtained by Ultrafast Camera and continuous LED light source.

5. Conclusions

Two out of the three planned experimental campaigns using the test rig by University of Manchester were conducted. These included a performance mapping exercise to investigate the flow physics in the domain, followed by a set of PIV measurements at selected test points. The following conclusions have been drawn:

1. The design of the scavenge suction source needs to be re-considered to enable more control of the scavenge mass flow via the split flow parameter, in particular at high inlet mass flow rates. This is in part due to the fixed design of the Venturi mass flow meter, and in part due to the fact that the core and scavenge suction sources are the same.
2. Separation efficiency measurements were delayed by a decision to first make improvements to the rig to achieve better control of the split flow parameter.
3. The rectangular cross-section of the 2.5D IPS does not lend itself well to high Reynolds number flows, thought to be due to the formation of vortices at the wall corners, which exacerbates flow separation and leads to a breakdown of the flow structure required for optimal particle separation.
4. More control of the split flow parameter is achieved at moderate Reynolds numbers, but this soon gives way to separated flow when inlet Reynolds number surpasses 100,000.
5. The PIV setup is capable of capturing the velocity field of two-thirds of the IPS fluid domain simultaneously, which will be especially useful for providing rich new insights into IPS flow physics.
6. The shadowgraphy setup enables the capability to investigate the particle size, shape, trajectory, velocity and rotation speed. A variety of camera and illumination systems were tested to compare their advantages.

6. Acknowledgments

This work was funded by an EU Horizon 2020 CleanSky2 award, ref. no. JTI-CS2-2017-CfP07-SYS-02-45.

7. References

[1] A. Filippone and N. Bojdo, “Turboshaft engine air particle separation,” *Prog. Aerosp. Sci.*, vol. 46, no. 5–6, pp. 224–245, 2010, doi: 10.1016/j.paerosci.2010.02.001.
[2] Kao, Y. H., Jiang, Z. W., & Fang, S. C. (2017). A Computational Simulation Study of Fluid Mechanics of Low-Speed Wind Tunnel Contractions. Fluids, 2(2), 23.
[3] Barone D., L. E. (2012). A 2-D Inertial Particle Separator Research Facility. Aerodynamic Measurement Technology, Ground Testing, and Flight Testing Conference. New Orleans: AIAA
[4] White, F. (2016). Fluid Mechanics. In F. White, Fluid Mechanics. McGraw-Hill Education.
[5] G. Fowles, W.H. Boyes, (2010) Chapter 6 - Measurement of Flow, Instrument Reference Book, 4th Ed., Butterworth-Heinemann